Chapter 4

Computational Study of Liquid Film Condensation with the Presence of Non-Condensable Gas in a Vertical Tube

Adil Charef, M'barek Feddaoui,
Abderrahman Nait Alla and Monssif Najim

Additional information is available at the end of the chapter

http://dx.doi.org/10.5772/intechopen.76753

Abstract

The main objective of this chapter is to study the liquid film condensation in a thermal desalination process, which is based on the phase change phenomenon. The external tube wall is subjected to a constant temperature. The set of the non-linear and coupled equations expressing the conservation of mass, momentum and energy in the liquid and gas mixtures is solved numerically. An implicit finite difference method is employed to solve the coupled governing equations for liquid film and gas flow together with the interfacial matching conditions. Results include radial direction profiles of axial velocity, temperature and vapour mass fraction, as well as axial variation of the liquid film thickness. Additionally, the effects of varying the inlet conditions on the phase change phenomena are examined. It was found that increasing the inlet-to-wall temperature difference improves the condensate film thickness. Decreasing the radius of the tube increased the condensation process. Additionally, non-condensable gas is a decisive factor in reducing the efficiency of the heat and mass exchanges. Overall, these parameters are relevant factors to improve the effectiveness of the thermal desalination units.

Keywords: thermal process, vapour-gas mixtures, condensation, heat and mass transfer, phase change

1. Introduction

The demand of fresh water supply is increasing due to the economic development and the fast population growth. With limited resources of fresh water, desalination of seawater and brackish water offers the potential to encounter the increasing water demands around the world. Generally, the reverse osmosis has about the great part of the market share in the world

compared to thermal desalination technologies. Consequently, the necessity to improve the thermal processes, which are based on the phase change phenomenon of evaporation and condensation, continues to receive a high interest. Condensation on the cooling surfaces is a phenomenon of major significance in the chemical industries, refrigeration, heat exchangers and desalination units, including thermal desalination.

The mechanism of condensation can be classified by various ways: geometric configurations like tube, channel, internal, external, horizontal or vertical; species of fluid such as steam, refrigerant or mixture with the presence of non-condensable gas; condensing phenomena as filmwise, dropwise or fog; and flow regime like laminar and turbulent. Since the first analysis of Nusselt [1] for film condensation on a vertical plate, a numerous number of studies have been done on improving film condensation modelling and to contribute to the comprehension of this complex phenomenon. Lebedev et al. [2] performed experimentally a combined study of heat and mass transfer from water vapour on a flat plate. They observed an enhancement of the condensation heat transfer with the increase of the inlet relative humidity. Dobran and Thorsen [3] studied the laminar filmwise condensation of a saturated vapour inside a vertical tube. They found that the mechanism of condensation is governed by ratio of vapour to liquid viscosity, Froude number to Reynolds number ratio, subcooling number and Prandtl number of liquid. Siow et al. [4, 5] presented a numerical study of the laminar film condensation with the presence of non-condensable gas in horizontal and then in vertical channels. They analysed the effect of the inlet Reynolds number, the inlet pressure and the inlet-to-wall temperature difference on the condensation mechanism. They studied also the liquid film condensation from steam-air mixtures inside a vertical channel. Results indicate that a higher concentration of non-condensable gas caused substantial reduces in the local Nusselt number, the pressure gradient and the film thickness. Belhadj et al. [6] conducted a numerical analysis to improve the condensation process of water vapour inside a vertical channel. Their results show that the phenomenon of phase change is sensitive to the inlet temperature of liquid film. For different values of the system parameters at the inlet of the tube, Dharma et al. [7] estimated from a numerical study the local and average values of Nusselt number, the pressure drop, the condensate Reynolds number and the gas-liquid interface temperature. Lee and Kim [8] carried out experimental and analytical studies to analyse the effect of the non-condensable gas (nitrogen) on the condensation of water vapour along a vertical tube with a small diameter. The experimental results demonstrate that the heat transfer coefficients become important with a high inlet vapour flow and the reduction of mass fraction of nitrogen. In addition, the authors developed a new correlation to evaluate the heat transfer coefficient regardless the diameter of the condenser tube. Nebuloni and Thome [9] developed a numerical and theoretical model to predict the laminar film condensation inside various channel shapes. They showed that the channel shape strongly affects the overall thermal performance. Chantana and Kumar [10] investigated experimentally and theoretically the heat transfer characteristics of steam-air during condensation inside a vertical tube. They observed that a higher Reynolds number and mass fraction of vapour improve the process of condensation. Dahikar et al. [11] conducted an experimental and CFD studies in the case of the film condensation with downward steam inside a vertical pipe. They found that a larger interfacial shear affects the momentum transfer because of the great velocity gradient especially at the gas-liquid interface.

http://dx.doi.org/10.5772/intechopen.76753

Merouani et al. [12] presented a numerical analysis during the condensation of steam-gas mixtures between two coaxial cylinders. They observed that a higher vapour concentration at the inlet and molar mass of the non-condensable gas increases the heat flux at the inner wall. Qiujie et al. [13] presented a numerical study in the case of steam-air condensation on isothermal vertical plate by using volume of fluid (VOF) method. Their results indicate that the mass fraction variation of the non-condensable gas directly affects the liquid film condensation and then influences the heat transfer.

In the thermal desalination unit, the condenser is used for producing freshwater from the saline water sources. In fact, in order to enhance the condensation process with the presence of non-condensable gas in thermal seawater desalination processes, many studies have been conducted. Semiat and Galperin [14] found from steam condensation that even a small air mass fraction decreases the heat transfer coefficient in seawater desalination plant. Al-Shammari et al. [15] have shown from an experimental study that non-condensable gas has a negative effect on the heat transfer. An experimental study on the role of non-condensable gases in the condensation of steam inside slightly inclined tubes was presented by Caruso et al. [16]. The experiments were carried out under the following conditions: inner diameter of the tube 12.6 and 26.8 mm, inclination of the tube 7°, mass fraction of the non-condensable gas between 5 and 42%, and vapour saturated at atmospheric pressure. Due to the gravity, the condensate is collected mainly in the lower part of the tube. They also developed a correlation to calculate the local condensation heat transfer coefficient. Hassaninejadfarahani et al. [17] investigated numerically a liquid film condensation with high amount of non-condensable gas inside vertical tube. They examined the effects of varying the inlet air mass fraction, the inlet relative humidity, the inlet Reynolds number and the radius of the tube on the simultaneous heat and mass transfer during condensation. Recently, Charef et al. [18] investigated the condensation process of water vapour-air into liquid film inside a vertical tube under two different boundary conditions: imposed temperature and imposed heat flux. The results indicated a better condensation process under imposed heat flux. It was found that the presence of non-condensable gas affects negatively the system efficiency.

The purpose of this study is to numerically develop and investigate the problem of water vapour condensation in the presence of non-condensable gas in a vertical tube. In order to improve the effectiveness of the steam condensation in desalination process, special attention is addressed to examine the effects of the tube geometry and the inlet conditions on the condensation process. In the following, we present the studied problem, the numerical method and the main results.

2. Mathematical model

2.1. Physical model and assumptions

The geometry under consideration is a vertical tube with length L and radius R (**Figure 1**). The tube wall is subjected to a constant temperature. A mixture of water vapour and non-

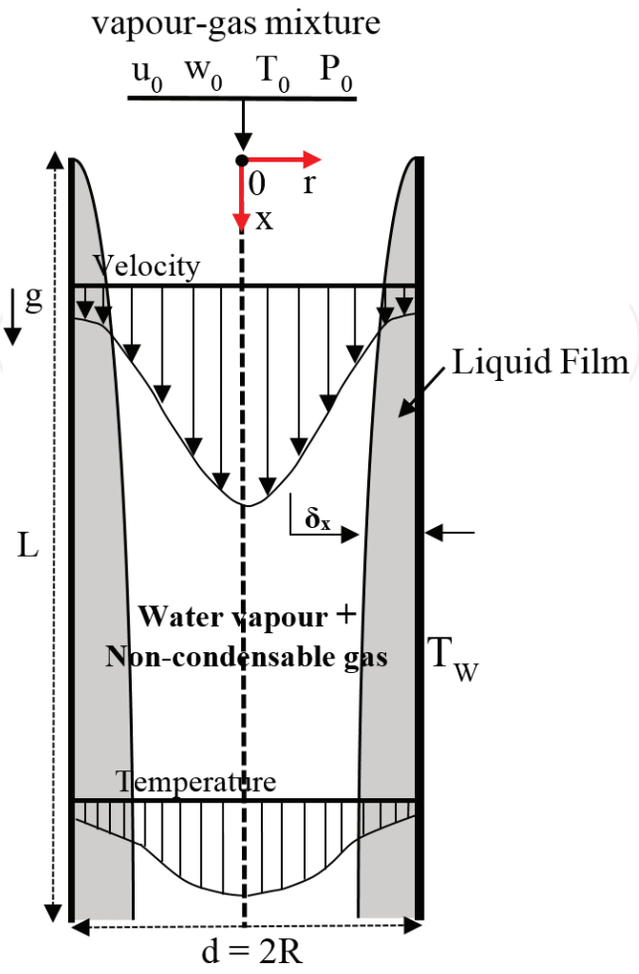

Figure 1. Geometry of the problem.

condensable gas enters the tube with a uniform velocity u_0, vapour mass fraction w_0, temperature T_0 and pressure P_0. The vapour condenses and forms a liquid film thickness as the mixture flowing downwards.

For the mathematical formulation of the problem, it has been assumed that the gas flow is laminar, incompressible and two-dimensional. The vapour and liquid phases are in thermodynamic equilibrium at the interface. In addition, viscous dissipation and other secondary effects are negligible, and the humid air is assumed to be a perfect gas.

2.2. Mathematical formulation

With respect to the mentioned assumptions, the governing equations for the conservation of mass, momentum and energy, respectively, in the liquid region are written as

- Conservation of mass:

$$\frac{\partial}{\partial x}(\rho_L u_L) + \frac{1}{r}\frac{\partial}{\partial r}(r\rho_L v_L) = 0 \tag{1}$$

http://dx.doi.org/10.5772/intechopen.76753

- Conservation of momentum:

$$\frac{\partial}{\partial x}(\rho_L u_L u_L) + \frac{1}{r}\frac{\partial}{\partial r}(r\rho_L v_L u_L) = -\frac{dp}{dx} + \frac{1}{r}\frac{\partial}{\partial r}\left(r\mu_L \frac{\partial u_L}{\partial r}\right) + \rho_L g \tag{2}$$

- Conservation of energy:

$$\frac{\partial}{\partial x}\left(\rho_L u_L C_{p,L} T_L\right) + \frac{1}{r}\frac{\partial}{\partial r}\left(r\rho_L v_L C_{p,L} T_L\right) = \frac{1}{r}\frac{\partial}{\partial r}\left(r\lambda_L \frac{\partial T_L}{\partial r}\right) \tag{3}$$

Similarly, the mass conservation, momentum, energy and diffusion equations for the gas phase are written as follows:

- Conservation of mass:

$$\frac{\partial}{\partial x}(\rho_G u_G) + \frac{1}{r}\frac{\partial}{\partial r}(r\rho_G v_G) = 0 \tag{4}$$

- Conservation of momentum:

$$\frac{\partial}{\partial x}(\rho_G u_G u_G) + \frac{1}{r}\frac{\partial}{\partial r}(r\rho_G v_G u_G) = -\frac{dp}{dx} + \frac{1}{r}\frac{\partial}{\partial r}\left(r\mu_G \frac{\partial u_G}{\partial r}\right) + \rho_G g \tag{5}$$

- Conservation of energy:

$$\frac{\partial}{\partial x}\left(\rho_G u_G C_{p,G} T_G\right) + \frac{1}{r}\frac{\partial}{\partial r}\left(r\rho_G v_G C_{p,G} T_G\right) = \frac{1}{r}\frac{\partial}{\partial r}\left(r\lambda_G \frac{\partial T_G}{\partial r}\right) \tag{6}$$

- Species diffusion equation:

$$\frac{\partial}{\partial x}(\rho_G u_G w) + \frac{1}{r}\frac{\partial}{\partial r}(r\rho_G v_G w) = \frac{1}{r}\frac{\partial}{\partial r}\left(r\rho_G D \frac{\partial w}{\partial r}\right) \tag{7}$$

2.3. Boundary and interfacial conditions

The governing equations are subjected to the following boundary conditions:

- At the tube inlet $(x = 0)$

$$u_G = u_0;\ T_G = T_0;\ P_G = P_0;\ \mathrm{w}_G = w_0 \tag{8}$$

- At the centre line of the tube $(r = 0)$

$$v_G = 0;\ \frac{\partial u_G}{\partial r} = \frac{\partial T_G}{\partial r} = \frac{\partial w}{\partial r} = 0 \tag{9}$$

- At the wall of the tube $(r = R)$

$$u_L = v_L = 0;\ T_L = T_W \tag{10}$$

- At the interface vapour-liquid $(r = R - \delta_x)$

Continuities of velocity and temperature:

$$u_I(x) = u_{G,I} = u_{L,I};\ T_I(x) = T_{G,I} = T_{L,I} \tag{11}$$

Continuity of shear stress:

$$\tau_I = \left[\mu \frac{\partial u}{\partial r}\right]_{L,I} = \left[\mu \frac{\partial u}{\partial r}\right]_{G,I} \tag{12}$$

Heat balance at the interface:

$$\lambda_L \frac{\partial T_L}{\partial r} = \lambda_G \frac{\partial T_G}{\partial r} - J^{''} h_{fg} \tag{13}$$

where h_{fg} is the latent heat of condensation and $J^{''}$ is the mass flux at the interface $\left(J^{''} = \rho_G v_I\right)$.

The radial velocity of water vapour-air mixture is calculated by considering that the interface is semipermeable [19] and that the solubility of air in the liquid film is negligibly small, which implies that the air velocity in the radial direction is zero at the interface. The velocity of the steam-air mixture at the interface can be written as

$$v_I = -\frac{\sum_{i=1}^{2} D_{G,im} \frac{\partial w_{Gi}}{\partial r}}{\left(1 - \sum_{i=1}^{2} w_{Gi}\right)} \tag{14}$$

The governing Eqs. (1)–(7) with interfacial conditions (8)–(13) are used to determine the field of variables u_L, v_L, T_L, u_G, v_G, T_G, w. To complete the mathematical model, two equations are used. At every axial location, the overall mass balance in the liquid phase and the gas flow should be satisfied:

$$\frac{m_{0L}}{2\pi} = \int_{R-\delta_x}^{R} (r\rho u dr)_L - \int_0^x \rho_G v_I (R - \delta_x) dx \tag{15}$$

$$\frac{(R - \delta_0)^2}{2} \rho_0 u_0 = \int_0^{R-\delta_x} (r\rho u dr)_G + \int_0^x \rho_G v_I (R - \delta_x) dx \tag{16}$$

A dimensionless accumulated condensation is introduced to estimate the mass transfer along the tube:

http://dx.doi.org/10.5772/intechopen.76753

$$m_{cd} = 2\pi \int_0^x \rho_G v_I (R - \delta_x) dx \tag{17}$$

A transformation of coordinates was performed to ensure that the computational grid would clearly define the gas-liquid interface at each station along the tube. The r, x coordinates are transformed into η, X as follows:

$$\eta = \frac{(R - \delta_x) - r}{(R - \delta_x)} \quad 0 \le r \le (R - \delta_x) \tag{18}$$

$$\eta = \frac{(R - \delta_x) - r}{\delta_x} \qquad (R - \delta_x) \le r \le R \tag{19}$$

$$X = \frac{x}{L} \tag{20}$$

The pure component data (in previous formulations) is approached by polynomials in terms of mass fraction and temperature. For more information, the thermo-physical properties are available in [20, 21].

3. Numerical solution method

The set of non-linear governing equations are discretized using a finite difference numerical scheme. The radial diffusion and the axial convection terms are approximated by the central and the backward differences, respectively. Hence, we arrange the system of discretized algebraic equations coupled with the boundary conditions into a matrix. Finally, the matrix resolution is carried out using the tri-diagonal matrix algorithm (TDMA) [22]. Besides that, a special care was made to ensure accuracy of the numerical computation, by generating a non-uniform grid in both directions. Accordingly, the grid is refined at the interface. In fact, it is important to note that as the liquid goes to the outlet, the film thickness varies along the tube. For that reason, during the downstream marching at each iteration, our finite difference computational grid deals with the variation of the liquid and gas computational domain.

3.1. Marching procedure

A set of non-linear algebraic equations is realized for $u_L, v_L, T_L, u_G, v_G, T_G, w$ and the two scalars dp/dx and δ_x. The computational solution is advanced as follows:

1. For any axial position x, guess an arbitrary values of dp/dx and δ_x.
2. Solve the finite difference forms of Eqs. (2)–(3) and (5)–(7) simultaneously for u_L, T_L, u_G, T_G, w.
3. Numerically, integrate the continuities of Eqs. (1) and (5) to find v_L and v_G.

4. The interfacial conditions of velocity, temperature, shear stress and heat balance are obtained from Eqs. (11)–(13).

5. Calculate the error of the liquid film mass balance E_L^{itt} using Eq. (15).

6. The best approximation to the thickness of the liquid film is then obtained using the secant method [23]. Thus

$$\delta_x^{itt+1} = \delta_x^{itt} - \frac{\delta_x^{itt} + \delta_x^{itt-1}}{E_L^{itt} - E_L^{itt-1}} E_L^{itt} \tag{21}$$

The convergence criteria used is $E_L^{itt} = 10^{-5}$. Usually, six to seven iterations suffice to get converged solution.

7. Calculate the error in the gas flow balance E_G^{itt} using Eq. (16).

8. Check the satisfaction of the convergence of velocity, temperature and species concentrations. If the relative error between two consecutive iterations is small enough, that is

$$E_{rr} = \frac{\max\left|\Upsilon_{i,j}^{n} - \Upsilon_{i,j}^{n-1}\right|}{\max\left|\Upsilon_{i,j}^{n}\right|} < 10^{-5} \tag{22}$$

The solution for the actual axial position is complete. If not, repeat procedures (1) to (7), where Υ represents the variables u_L, T_L, u_G, T_G, w.

3.2. Velocity and pressure coupling

Owing to satisfy the global mass flow constraint, the pressure correction gradient and axial velocity profile are performed applying a method proposed by Raithby and Schneider [24], described by Anderson et al. [25]. To fully explain, we let $H = {}^{dp}/_{dx}$. Due to an initial guesses for $(-{}^{dp}/_{dx}) = (-{}^{dp}/_{dx})^*$, we calculate provisional velocities $\left(u_j^{n+1}\right)^*$ and a mass flow rate of gas $\left(\dot{M}_j^{n+1}\right)^*$. Because of the linearity of the equation of momentum with frozen coefficients, the correct velocity at each point from an application of Newton's method is as follow:

$$u_j^{n+1} = \left(u_j^{n+1}\right)^* + \frac{\partial u_j^{n+1}}{\partial H} \Delta H \tag{23}$$

ΔH is the change in the gradient of the pressure required to satisfy the global mass flow constraint. In addition, we specify $u_{p,j}^{n+1} = \frac{\partial u_j^{n+1}}{\partial H}$. The difference equations are indeed differentiated with respect to the pressure gradient (H) to have difference equations for $u_{p,j}^{n+1}$, which have a tridiagonal form. The coefficients for the unknowns in these equations will be the same as for the original implicit difference equations. The system of algebraic equations for $u_{p,j}^{n+1}$ is

http://dx.doi.org/10.5772/intechopen.76753

resolved by Thomas algorithm. Furthermore, the boundary conditions on $u_{p,j}^{n+1}$ must be coherent with the boundary conditions of the velocity. At boundaries, where the velocity is specified, $u_{p,j}^{n+1} = 0$. The solution of $u_{p,j}^{n+1}$ is used to calculate ΔH, noting that to satisfy the constraint of the global mass flow, $u_{p,j}^{n+1}\Delta H$ is the correction in velocity at each point. So, we can write

$$\dot{M}_i^{n+1} - \dot{M}_i^n = 2\pi\Delta H \int_0^{R-\delta_x} r\rho u_{p,j}^{n+1} dr \tag{24}$$

where the integral is estimated using numerical means. The $\dot{M}_i^{n+1}$ in Eq. (24) is the known value specified in the initial conditions. The required value of ΔH is given by Eq. (24), whereas the correct values of the velocity u_j^{n+1} may be determined from Eq. (23). Besides, the continuity equation then allows to calculate v_j^{n+1}.

3.3. Mesh stability and validation of the numerical model

To validate the grid independency of results and to avoid convergence problems due to the use of thin grids, it is helpful to choose an optimum solution between computational time and result precision. Several grid sizes have been examined to ensure that the results are grid independent. **Figure 2** shows that in all grid arrangements, the difference in local Nusselt number of sensible heat is always less than 3%. The grid with $NI \times (NJ + NL) = 131 \times (81 + 31)$ is chosen because it gives results close enough to those of the thin grid and sufficiently accurate

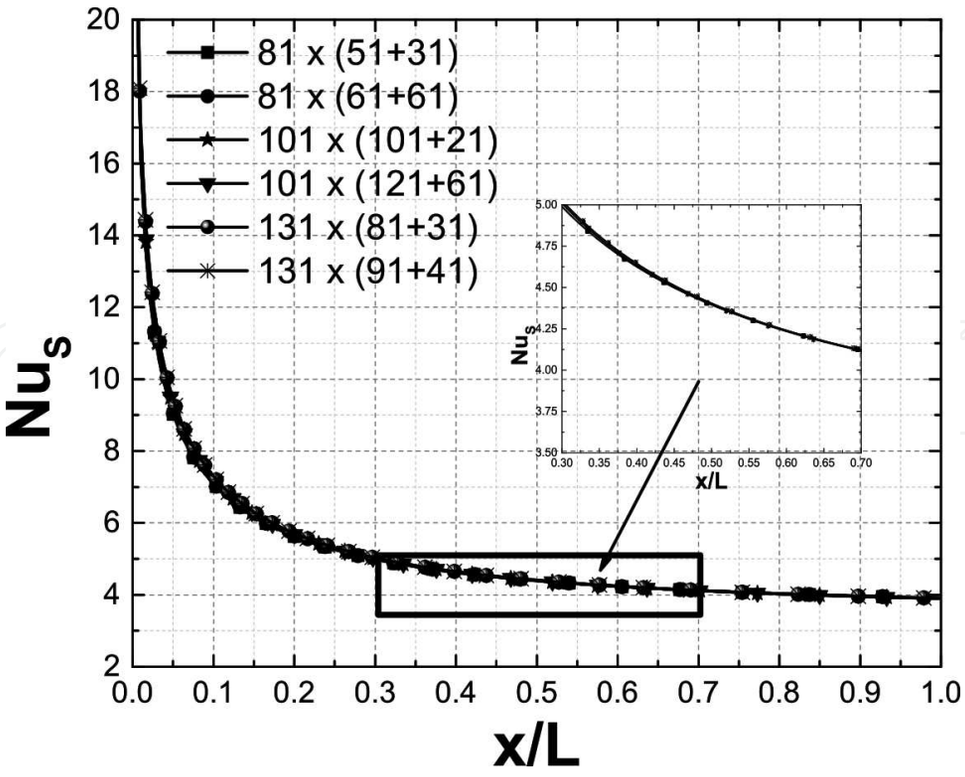

Figure 2. Comparison of sensible heat Nusselt number.

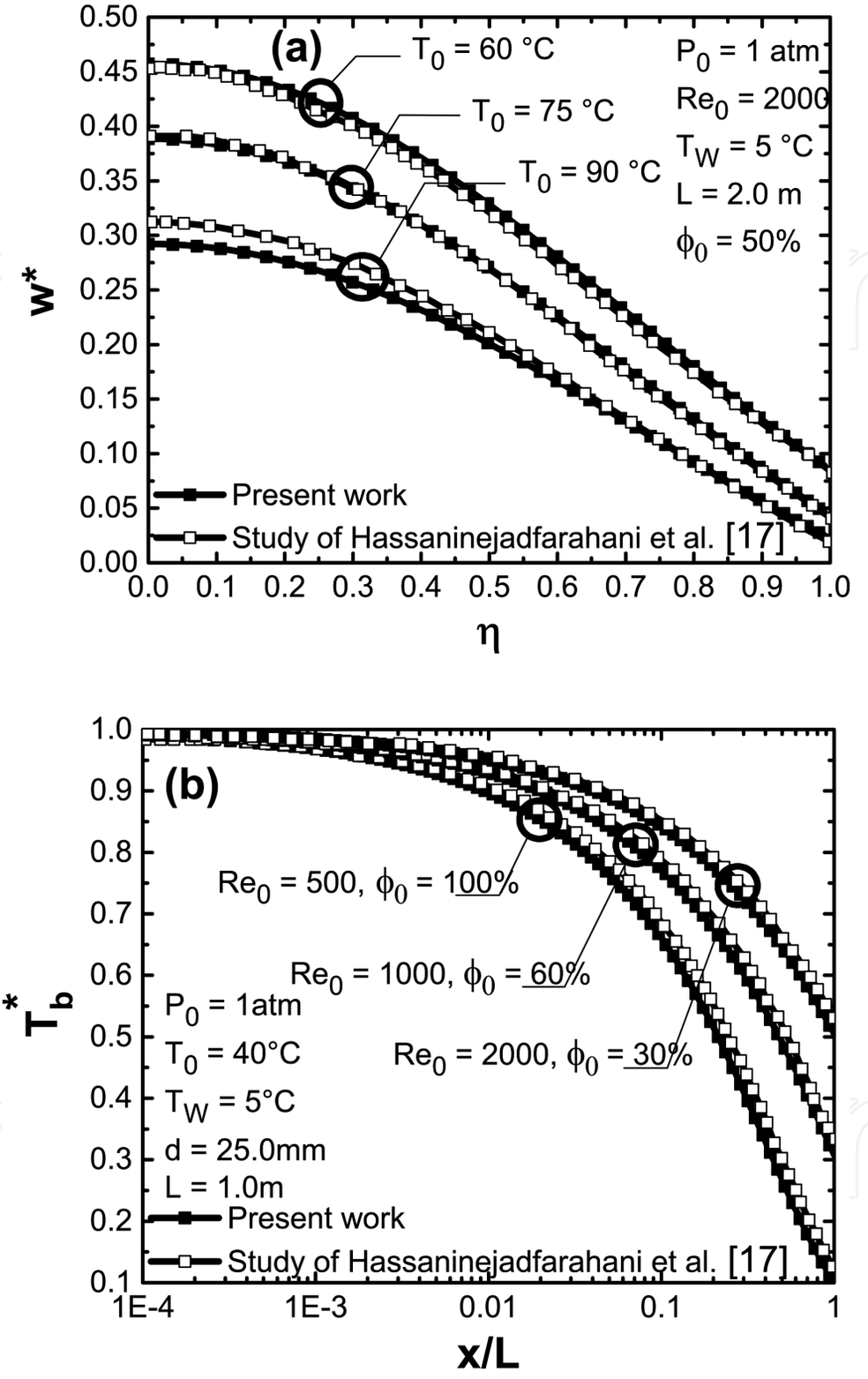

Figure 3. Comparison with numerical study of Hassaninejadfarahani et al. [17] for (a) dimensionless mass fraction at the tube exit, and (b) dimensionless mixture temperature.

to describe the heat and mass transfer. Note that *NI* is the total grid points in the axial direction, *NJ* is the total grid points in the radial direction at the gas region, and *NL* is the total grid points in the radial direction at the liquid region.

http://dx.doi.org/10.5772/intechopen.76753

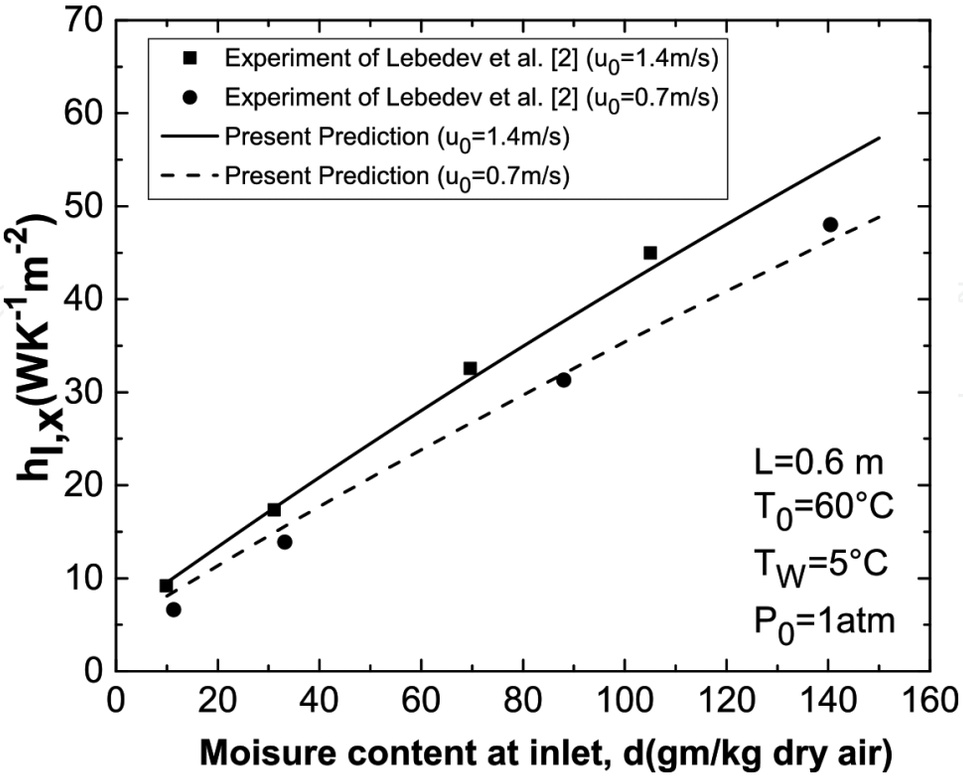

Figure 4. Comparison with experimental data of Lebedev et al. [2] for local condensate heat transfer coefficient.

In order to check the accuracy and validity of the numerical method, the obtained results were first compared to those reported by Hassaninejadfarahani et al. [17] in the case of laminar condensation of a steam and non-condensable gas in a vertical tube, in which the tube wall is maintained at a constant temperature. A good agreement was found between the current computational study and the results provided by Hassaninejadfarahani et al. [17] as shown in **Figure 3a**, **b**, which illustrates the vapour mass fraction evolution and mixture temperature, respectively.

The computations have been also compared with experimental results of Lebedev et al. [2]. It is important to indicate that Lebedev et al. [2] examined the simultaneous heat and mass transfer during humid air condensation in a vertical duct. So, to obtain the case of Lebedev et al. [2], equivalent hydraulic diameter *de* is chosen [7, 26]. **Figure 4** is a plot of local condensate heat transfer coefficient compared with the study of Lebedev et al. [2] for T_0 = 60°C, P_0 = 1 atm, L = 0.6 m, T_W = 5°C and de = 0.02 m. A good agreement between our computations and the experiment curves is found with a maximum relative error of 4.7% for both curves (u_0 = 1.4 m/s and u_0 = 0.7 m/s).

4. Distribution of axial velocity, temperature and mass fraction profiles along the vertical tube

This chapter investigates the process of the liquid film condensation from the water vapour and non-condensable gas mixtures inside a vertical tube. The results of this study have been

obtained for the case of inlet gas temperature T_0=70°C, inlet pressure P_0=1 atm and inlet Reynolds number is fixed at Re_0 = 2000. The range of each parameter for this study is listed in **Table 1**. At first, the air is used as non-condensable gas.

Figures 5–7 Illustrate the profiles of velocity, temperature and the mass fraction of water vapour at different axial locations of the tube. From the distribution of velocity in **Figure 5**, it is observed that the variation of the velocity in the gas mixture is higher than that in the liquid region. Moreover, as the gas flow progresses along the tube, the velocity in the mixture decreases, while the velocity in the liquid film slightly rises. This behaviour is due to the mass transfer from the mixture to the liquid film. In fact, when the gas mixture loses the mass, it loses velocity too, however, the liquid film gaining mass as well as acceleration. **Figure 6** Presents the evolution of the temperature profiles in both mixture and liquid phases at different tube sections. It can be seen that in the liquid phase, the temperature profiles are close to the temperature of the wall and nearly linear. This indicates that the interface temperature

Tube length (L (m))	3.0, 4.5, 6.0
Tube radius (R(m))	0.008, 0.01, 0.012
Inlet vapour mass fraction (w_0)	0.05, 0.125, 0.2
wall temperature (T_W(°C))	5, 20, 35
Non-condensable gas	Oxygen, air, nitrogen

Table 1. The ranges of the physical parameters.

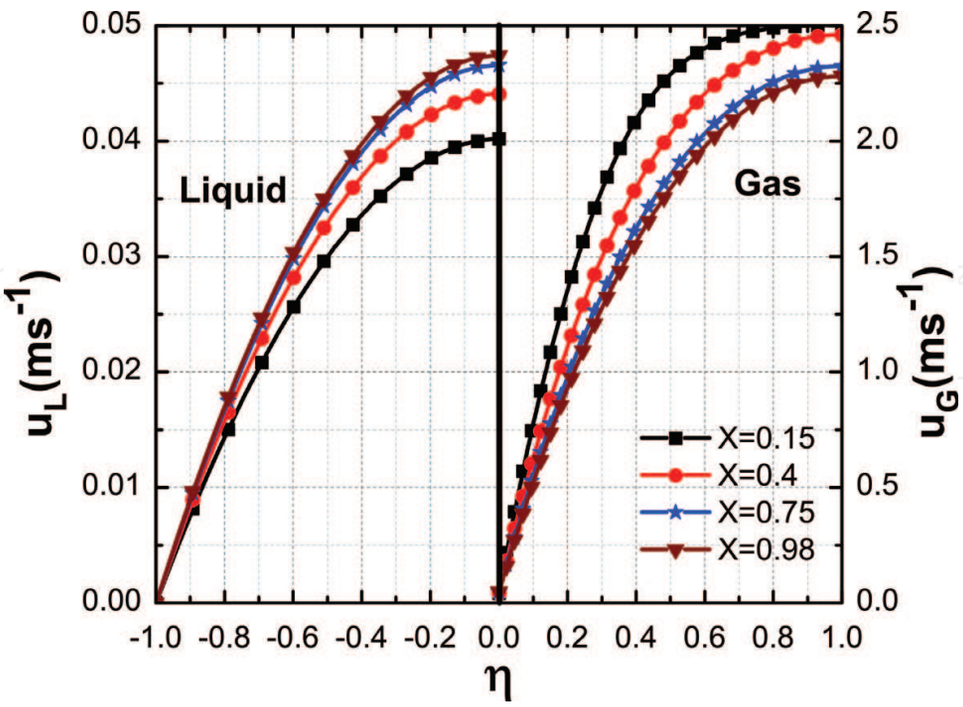

Figure 5. Distributions of axial velocity profile in both the liquid and vapour phases at different tube sections.

http://dx.doi.org/10.5772/intechopen.76753

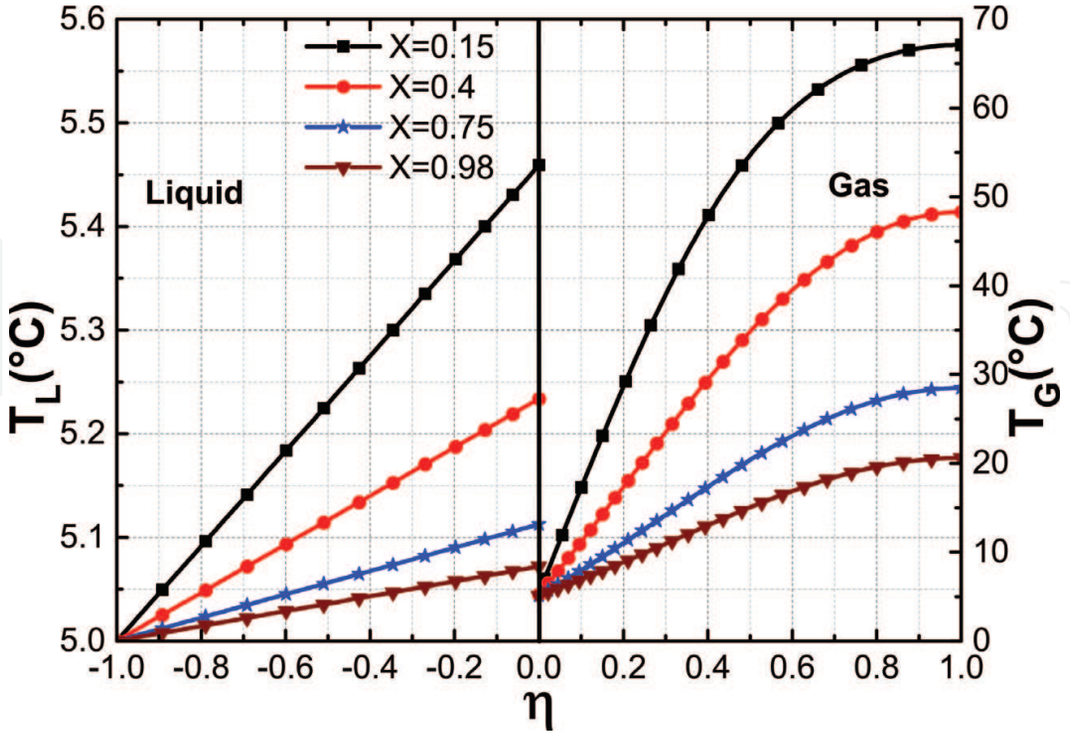

Figure 6. Distributions of axial temperature profile in both the liquid and vapour phases at different tube sections.

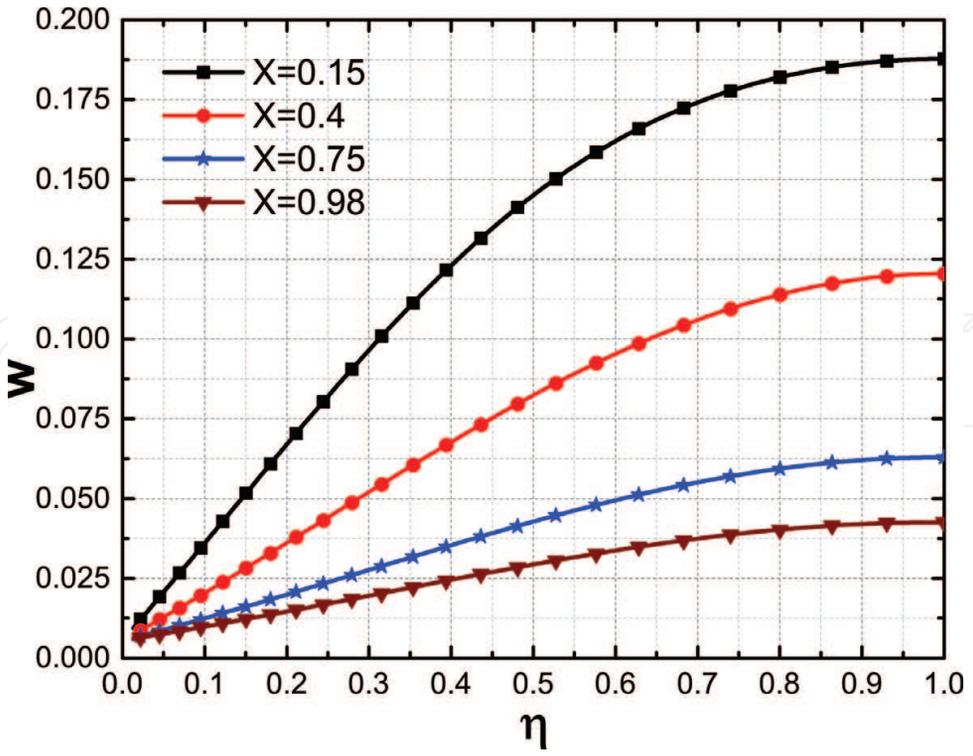

Figure 7. Distributions of axial vapour mass fraction profile in gas phases at different tube sections.

decreases from the inlet to the tube exit, resulting in the reduction of the heat transfer across the condensate film. Also, the slopes of the temperature of the mixture are decreasing along the tube owing to the absorbed energy transferred from the gas flow to the liquid film. The distributions of the mass fraction of water vapour in the gas region are illustrated in **Figure 7**. It is interesting to observe that the vapour mass fraction w_0 decreases from the entrance to the tube exit, which implies that the condensation rate is decreasing along the tube. Consequently, w_0 is reduced from the Centre line ($\eta = 1$) to the liquid-vapour interface ($\eta = 0$).

5. Effect of the tube geometry (length *L* and radius *R*)

In the desalination units, the tube geometry of which the water vapour condenses (whether it is the length or the radius) contributes positively to the improvement of the condensation process if they are well dimensioned.

To reveal their impacts, we first examined the impact of the length of the tube on the liquid film thickness and the condensing mass flux at the interface along the tube. **Figure 8** shows the influence of the tube length on the thickness of the film and condensing mass flux at the interface. It is noted that δ_x increases with increasing the tube length L. The results also indicate that, for a high tube length, the mechanism of the condensation is important when the distance is less than ($X = 0.8$), especially for $L = 4.5$ m and 6.0 m, because for a fixed Reynolds gas number (the inlet velocity is fixed too), the condensed vapour decreases with the increase of tube length. This means that near to the tube exit, the condensation process becomes almost unimportant. It is

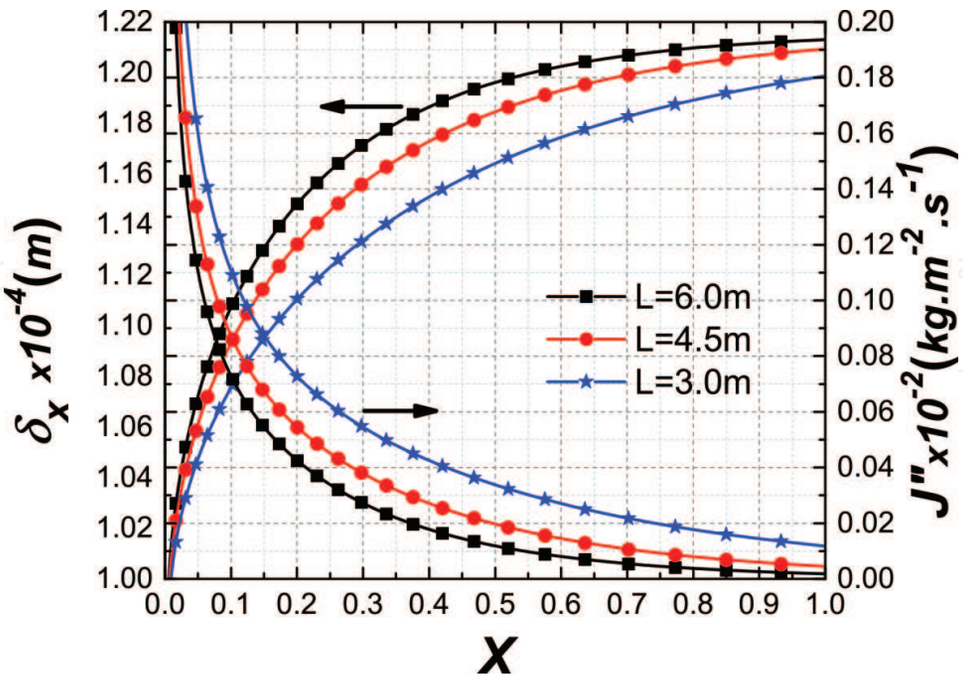

Figure 8. Effect of the tube length on the variation of the liquid film thickness and the condensing mass flux at the interface along the tube.

http://dx.doi.org/10.5772/intechopen.76753

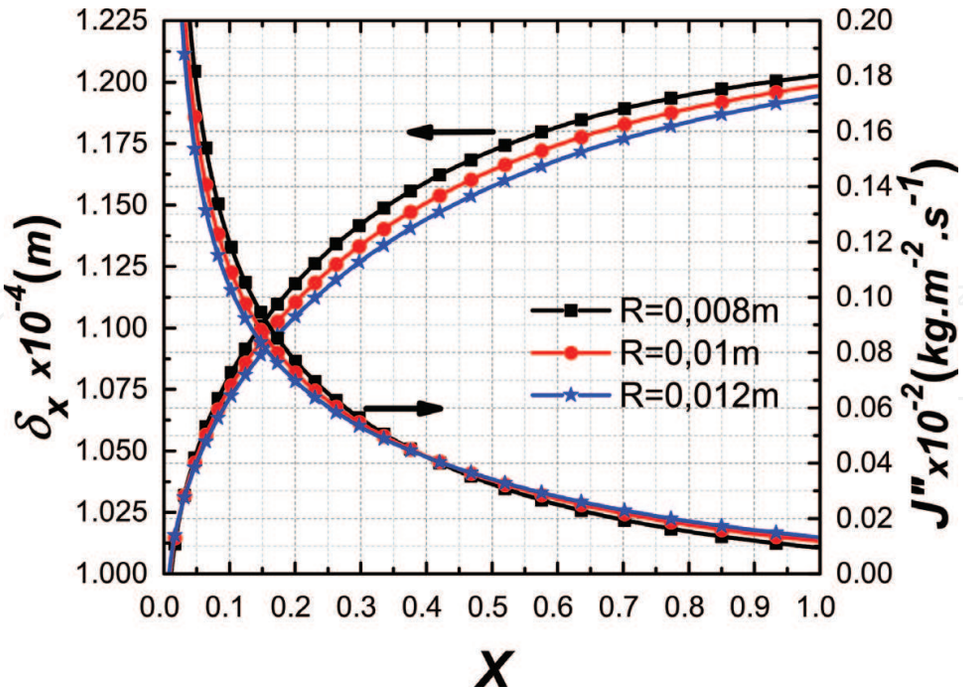

Figure 9. Effect of the tube radius on the variation of the liquid film thickness and the condensing mass flux at the interface.

also observed that the condensing mass flux reduces from the inlet to the outlet, particularly for the two large values of L approaching zero, because the total amount of the water vapour is transferred to liquid film and remains only the air at the vapour-liquid interface.

The effect of changing the tube radius R is shown in **Figure 9**. From the curves in this figure, it is interesting to observe that for a fixed value of T_0, w_0 and Re_0, a smaller tube radius corresponds to a thicker liquid film thickness. This trend is true for every position X from the inlet to the outlet of the tube. These results are directly related to the velocity of the gas mixture at the inlet. Obviously, for a fixed Reynolds number, δ_x increases according to the velocity increases with a weak tube radius. This implies that a higher inlet velocity tends to move the air away from the interface and thus maintains its lower fraction, leading to the increase of the heat transfer coefficient, which improves the condensation process. It is also found that the condensing mass flux increases with the tube radius only near the inlet when $X < 4$ due to a high interfacial shear stress. This tendency is reversed as the gas mixture progresses along the tube.

6. Effect of water vapour mass fraction w_0

In the majority of thermal desalination units, the water vapour that does not condense at the first effect, with all the non-condensable gases content, is transferred to the second effect, and this produces gas accumulation up to inadmissible concentrations. These gases cause a reduction in the performance of the system.

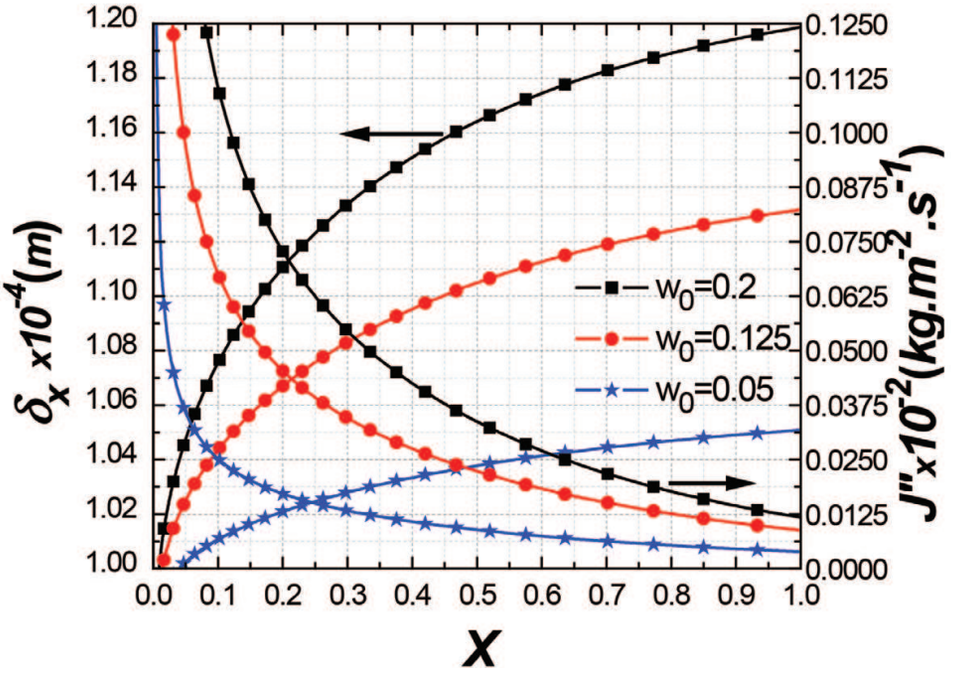

Figure 10. Effect of the inlet vapour mass fraction on the variation of the liquid film thickness and the condensing mass flux at the interface.

This result is confirmed in **Figure 10**, which shows that the thickness of the film increases considerably from the inlet to the exit of the tube. It is also observed that the increase in the mass fraction of water vapour w_0 considerably improves the condensation mechanism along the tube. Indeed, for a constant T_0, an increase of w_0 affects the thermo-physical properties of the gas mixture at the inlet, which leads to an augmentation of the vapour partial pressure and the temperature at the vapour-liquid interface. Consequently, the condensing mass flux at the interface J'' increases significantly with w_0 leading to an increase in the rate of condensation, which improves the thickness of the liquid film. On the other hand, a small amount of w_0 (inversely proportional to the mass fraction of the non-condensable gas) causes a remarkable reduction of the condensed mass flux rate and the axial variation of the thickness of the film along the tube. This is due to the presence of air, which plays the role of thermal and mass transfer resistance at the vapour-liquid interface.

7. Effect of the wall temperature T_W

The effect of the wall temperature T_W on the liquid film thickness and the condensing mass flux is presented in **Figure 11**. It is noted that the thickness of the liquid film varies inversely with the imposed temperature of the wall. Clearly, there is a significant growth of the liquid film thickness when T_W reduces from 35°C to 5°C because the amount of the condensed vapour is enhanced along the tube by the increase of the heat transfer and hence the thickness of the

http://dx.doi.org/10.5772/intechopen.76753

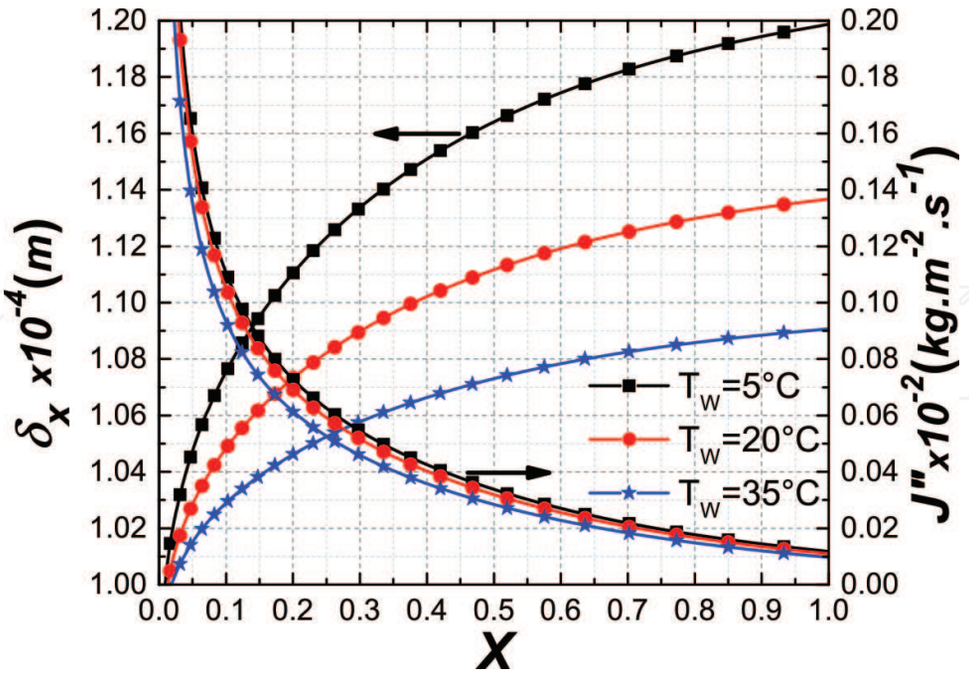

Figure 11. Effect of T_W on the evolution of the liquid film thickness and the condensing mass flux at the interface.

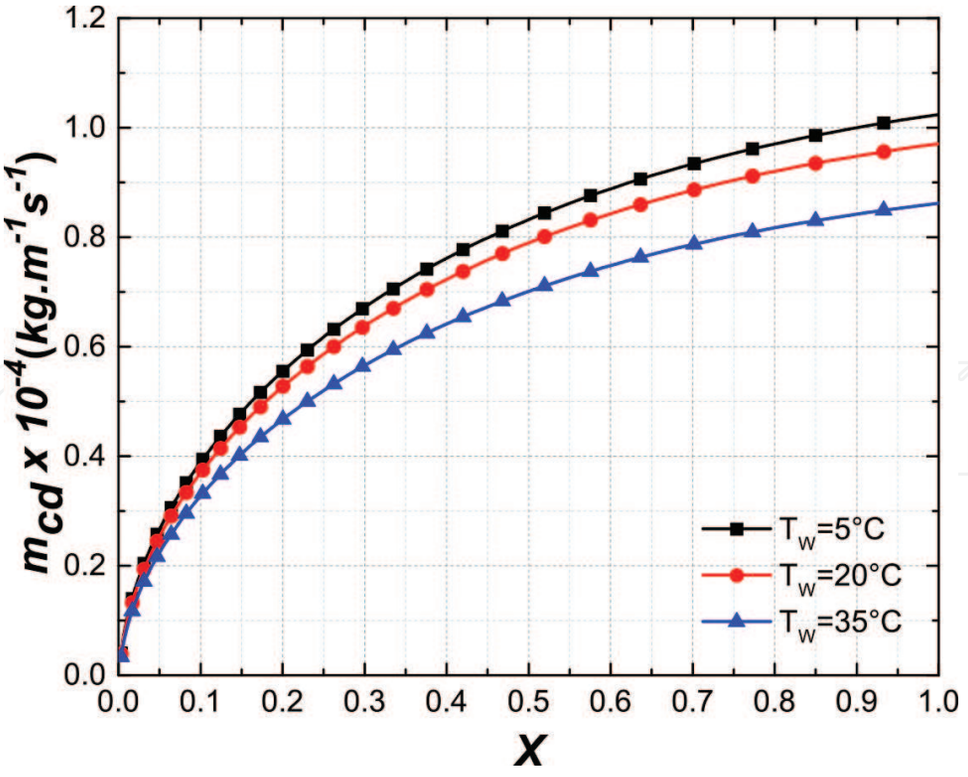

Figure 12. Effect of T_W on the accumulated condensation along the tube.

liquid film becomes thicker. From this figure, it is also observed that the condensing mass flux is important for a large value of the inlet-to-wall temperature difference and then decreases along the tube. The results indicate that J'' decreases as the gas flow progresses along the tube because the condensation is accompanied by a diminution in the temperature of the vapour phase and the heat transferred by the latent mode during the condensation to the liquid film. The effect of wall temperature on the accumulated condensation m_{cd} is illustrated in **Figure 12**. It can be seen that m_{cd} becomes important for low temperatures. When the temperature difference (T_0 - T_W) increases, the heat transfer increases, and consequently the density of the condensed flux increases. This explains why the condensation process is favoured for a higher-temperature difference.

8. Effect of the non-condensable gas type

In thermal desalination units, when the water vapour condenses, the presence of a non-condensable gas hinders this phenomenon. The accumulation of non-condensable components at the vapour-liquid interface plays the role of an obstacle for heat and mass transfer. This causes a reduction in the efficiency of the system and therefore an increase in costs in most desalination units using phase change.

In this section, we analyse the influence of the non-condensable gas type during water vapour condensation. We considered mixed mixtures of water-oxygen, water-air and water- nitrogen. The molar mass of oxygen, air and nitrogen are equal to 31.99, 28.95 and 28.01 g/mol, respectively. Since the liquid film thickness δ and the condensing mass flux at the interface J'' determine the condensation efficiency, **Figure 13** illustrates the variation of δ and J'' along the

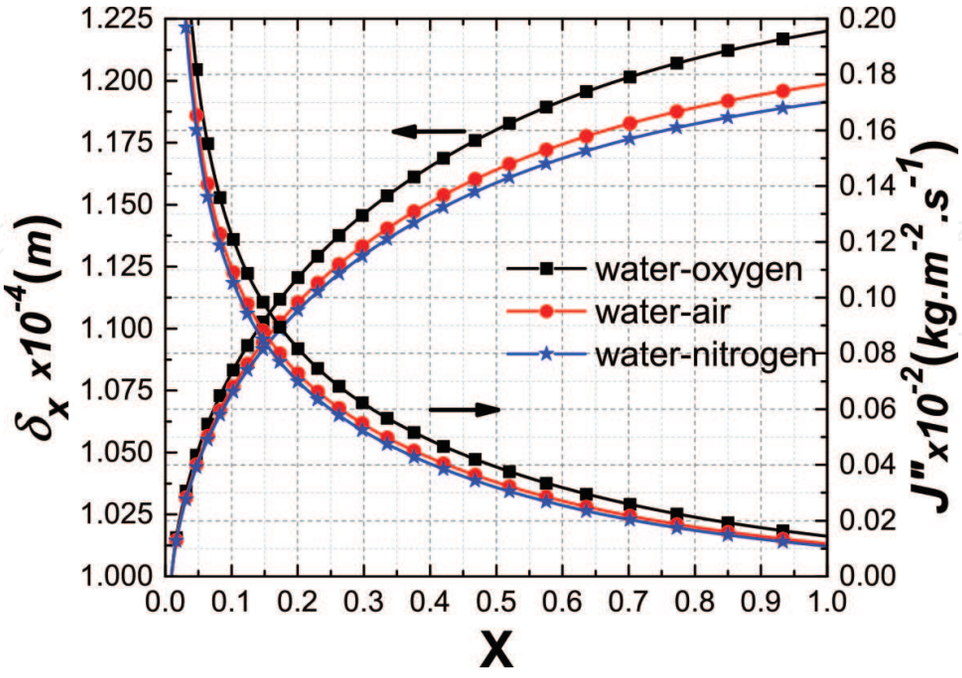

Figure 13. Effect of the type of non-condensable gas on the evolution of the liquid film thickness and the condensing mass flux at the interface along the tube.

http://dx.doi.org/10.5772/intechopen.76753

tube. For a fixed w_0, P_0 and Re_0, an increase in the molar mass of the gas leads to a growth in the density of the gas mixture, the temperature of the gas mixture, as well as a decrease in the saturation concentration especially for water-oxygen mixture. This causes a strong vapour concentration gradient and condensing mass flux at the vapour-liquid interface. The results obtained show that the evolution of the film thickness and condensing mass flux in the water-oxygen mixture are significantly greater than those of the other mixtures. In addition, the condensing mass flux decreases along the tube and tends to a lower value especially near to the tube exit, which means the end of the condensation process.

9. Conclusion

A numerical analysis has been carried out to investigate the liquid film condensation of the water vapour with the presence of non-condensable gas inside a vertical tube. The main conclusions drawn from this study are as follows:

1. The efficiency of the system is enhanced by increasing the tube length and decreasing the radius, which allows condensing the maximum of the water vapour.
2. A small amount of non-condensable gas improves the heat and mass exchanges.
3. Decreasing the wall temperature enhances the liquid film thickness and the accumulated condensation.
4. The non-condensable gas type has a great effect on the condensation process.

Nomenclature

Cp	specific heat (J. kg^{-1}. K^{-1})
D	diffusion coefficient (m^2. s^{-1})
d	diameter of the tube (m)
R	radius of the tube (d/2) (m)
L	tube length (m)
g	gravitational acceleration (m. s^{-2})
Nus	sensible Nusselt number
m_{cd}	accumulated condensation
P	atmospheric pressure (Pa)
T	temperature (°C)
u	axial velocity (m. s^{-1})

v radial velocity (m. s^{-1})

w mass fraction of vapour

J″ mass flux at the interface ($kg.m^{-2}.s^{-1}$)

h_{fg} latent heat of condensation (J. kg^{-1})

r radial coordinate (m)

Greek symbols

δ liquid film thickness (m)

λ thermal conductivity ($w.k^{-1}$. m^{-1})

μ dynamic viscosity (kg. m^{-1}. s^{-1})

ρ density (kg. m^{-3})

τ shear stress

ϕ relative humidity (%)

Subscripts

L referring to the liquid

G referring to the gas mixture

I interface

0 condition at inlet of the tube

W condition at wall of the tube

a referring to the air

x axial

Author details

Adil Charef*, M'barek Feddaoui, Abderrahman Nait Alla and Monssif Najim

*Address all correspondence to: adil.charef@edu.uiz.ac.ma

Laboratory of Energy, Materials and Systems Engineering, Ibn Zohr University, Agadir, Morocco

References

[1] Nusselt W. Die Oberflachenkondesation des Wasserdamffes the surface condensation of water. Zetrschr. Ver. Deutch. Ing. 1916:541-546

[2] Lebedev PD, Baklastov AM, Sergazin ZF. Aerodynamics, heat and mass transfer in vapour condensation from humid air on a flat plate in a longitudinal flow in asymmetrically cooled slot. International Journal of Heat and Mass Transfer. 1916;**12**:833-841. DOI: 10.1016/0017-9310(69)90150-1

[3] Dobran F, Thorsen RS. Forced flow laminar filmwise condensation of a pure saturated vapor in a vertical tube. International Journal of Heat and Mass Transfer. 1980;**23**:161-177. DOI: 10.1016/0017-9310(80)90194-5

[4] Siow E, Ormiston S, Soliman H. Fully coupled solution of a two-phase model for laminar film condensation of vapor-gas mixtures in horizontal channels. International Journal of Heat and Mass Transfer. 2002;**45**(18):3689-3702

[5] Siow E, Ormiston S, Soliman H. A two-phase model for laminar film condensation from steam air mixtures in vertical parallel-plate channels. Heat and Mass Transfer. 2004;**40**(5): 365-375

[6] Belhadj Mohamed A, Orfi J, Debissi C, Ben Nasrallah S. Condensation of water vapor in a vertical channel by mixed convection of humid air in the presence of a liquid film flowing down. Desalination. 2007;**204**:471-481

[7] Dharma Rao V, Murali Krishna V, Sharma K, Rao PM. Convective condensation of vapor in the presence of a non-condensable gas of high concentration in laminar flow in a vertical pipe. International Journal of Heat and Mass Transfer. 2008;**51**:6090-6101

[8] Lee KY, Kim MH. Experimental and empirical study of steam condensation heat transfer with a noncondensable gas in a small-diameter vertical tube. Nuclear Engineering and Design. 2008;**238**:207-216. DOI: 10.1016/j.nucengdes.2007.07.001

[9] Nebuloni S, Thome JR. Numerical modeling of laminar annular film condensation for different channel shapes. International Journal of Heat and Mass Transfer. 2010;**53**:2615-2627. DOI: 10.1016/j.ijheatmasstransfer.2010.02.054

[10] Chantana C, Kumar S. Experimental and theoretical investigation of air-steam condensation in a vertical tube at low inlet steam fractions. Applied Thermal Engineering. 2013;**54**: 399-412. DOI: 10.1016/j.applthermaleng.2013.02.024

[11] Dahikar SK, Ganguli AA, Gandhi MS, Joshi JB, Vijayan PK. Heat transfer and flow pattern in co-current downward steam condensation in vertical pipes-I: CFD simulation and experimental measurements. The Canadian Journal of Chemical Engineering. 2012:1-15

[12] Merouani L, Zeghmati B, Belhamri A. Numerical modelling of convective vapour condensation with non-condensable gases between two coaxial vertical cylinders. The Canadian Journal of Chemical Engineering. 2013;**91**:1597-1607

[13] Qiujie Y, Tian M, Fang D. CFD simulation of air-steam condensation on an isothermal vertical plate. International Journal of Heat and Technology. 2015;**33**:25-32. DOI: 10.18280/ijht.330104

[14] Semiat R, Galperin Y. Effect of non-condensable gases on heat transfer in the tower MED seawater desalination plant. Desalination. 2001;**140**(1):27-46

[15] Al-Shammari S, Webb D, Heggs P. Condensation of steam with and without the presence of non-condensable gases in a vertical tube. Desalination. 2004;**169**(2):151-160 http://dx.doi.org/10.1016/j.desal.2003.11.006

[16] Caruso G, Di Maio DV, Naviglio A. Condensation heat transfer coefficient with non-condensable gases inside near horizontal tubes, Desalination, vol. 309, (2013) pp. 247-253. DOI: 10.1016/j.ijheatmasstransfer.2013.09.049

[17] Hassaninejadfarahani F, Guyot MK, Ormiston S. Numerical analysis of mixed-convection laminar film condensation from high air mass fraction steam–air mixtures in vertical tubes. International Journal of Heat and Mass Transfer. 2014;**78**:170-180. DOI: 10.1016/j.ijheatmasstransfer.2014.06.047

[18] Charef A, Feddaoui M, Najim M, Meftah H. Liquid film condensation from water vapour flowing downward along a vertical tube. Desalination. 2017;**409**:21-31. DOI: 10.1016/j.desal.2017.01.018

[19] Eckert E, Drake Jr. Analysis of Heat and Mass Transfer. New York: Hemisphere Publishing; 1987

[20] Poling BE, Prausnitz JM, John Paul O, Reid RC. The Properties of Gases and Liquids, 5. New York: McGraw-Hill; 2001

[21] Perry R, Green D. Perrys Chemical Engineers Handbook. New York: McGraw-Hill; 1997

[22] Patankar S. Numerical Heat Transfer and Fluid Flow. New York: Hemisphere/McGraw-Hill; 1980

[23] Nougier JP. Méthodes de calcul numérique. 3rd ed. Paris: Masson; 1991

[24] Raithby GD, Schneider GE. Numerical solution of problems in incompressible fluid flow: Treatment of the velocity pressure coupling. Numerical Heat Transfer. 1979;**2**(4):417-440

[25] Anderson DA, Tannehill JC, Pletcher RH. Computational Fluid Mechanics and Heat Transfer. New York: Hemisphere/McGraw-Hill; 1984

[26] Charef A, Feddaoui M, Najim M, Meftah H. Comparative study during condensation of R152a and R134a with presence of non-condensable gas inside a vertical tube. Heat and Mass Transfer. 2018;**54**:1085-1099. DOI: 10.1007/s00231-017-2205-2